Thermochimica Acta, 114 (1987) 209–225
Elsevier Science Publishers B.V., Amsterdam – Printed in The Netherlands

THERMAL DECOMPOSITION OF ENERGETIC MATERIALS. 20. A COMPARISON OF THE STRUCTURAL PROPERTIES AND THERMAL REACTIVITY OF AN ACYCLIC AND CYCLIC TETRAMETHYLENETETRANITRAMINE PAIR

Y. OYUMI, T.B. BRILL * and A.L. RHEINGOLD
Department of Chemistry, University of Delaware, Newark, DE 19716 (U.S.A.)
(Received 18 August 1986)

ABSTRACT

The linear secondary nitramine, 1,7-dimethyl-1,3,5,7-tetranitrotrimethylenetetramine $CH_3[N(NO_2)CH_2]_3N(NO_2)CH_3$ (OHMX) and its cyclic analog, octahydro-1,3,5,7-tetranitro-1,3,5,7-tetrazocine, $(CH_2NNO_2)_4$ (HMX) are compared. By IR spectroscopy and DTA, OHMX is found to exist in five polymorphs between 273 K and its melting point at 490 K. The IR spectra suggest that the structural differences involve mostly the NO_2 and CH_3 groups and changes in lattice symmetry without a significant alteration in the conformation of the backbone. The kinetic parameters for the OHMX(III → IV) phase transition are first order ($E_a = 50.8$ kcal mol^{-1}) and are comparable to those of HMX. The nucleation process is probably being measured. The values of ΔH for the phase transitions of OHMX (0.8–2.1 kcal mol^{-1}) are also similar to those of HMX. The molecular structure of OHMX(II) was determined: monoclinic, $P2_1/c$, $a = 20.952(7)$, $b = 9.477(2)$, $c = 6.521(2)$ Å, $\beta = 96.29(3)°$, $Z = 4$, $D_{calc} = 1.598$ g cm^{-3}, $R_F = 3.84$, $R_{wF} = 4.68\%$. It consists of a helical chain of CH_2NNO_2 units staggered at approximately 120° intervals. A pseudo-C_2 axis is present. OHMX is slightly less thermally stable than HMX. High-rate thermolysis ($dT/dt = 110$ K s^{-1}) of OHMX liberates products that are the same, with a few exceptions, as for HMX. Competitive N–N and C–N bonds fission occurs as predicted by the IR data and molecular structure. The pressure dependence of the decomposition process indicates that the heterogeneous gas-condensed phase reactions occur to a greater extent as the pressure increases.

INTRODUCTION

Cyclization is a fundamental variable whose influence needs to be tested in the quest to understand how the molecular structure, properties, and subsequent thermolytic reactivity of molecules are connected. Cyclic and acyclic molecules have not been compared in these studies [1]. Addressed in this paper is a comparison of the structural details and thermal decomposition of the cyclic secondary nitramine, 1,3,5,7-tetranitro-1,3,5,7-tetrazocine

* Author for correspondence.

0040-6031/87/$03.50

(HMX), and the analogous linear tetrazanitramine, 1,7-dimethyl-1,3,5,7-tetranitrotrimethylenetetramine (OHMX). It is not possible to prepare perfectly analogous linear and cyclic nitramine pairs because of the necessity of providing a chain terminus for the linear nitramine. However, the essential compositional features are repeated in HMX and OHMX.

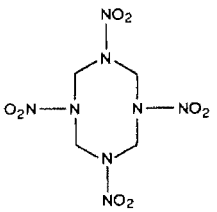

HMX

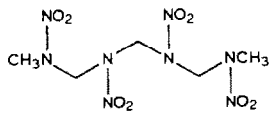

OHMX

HMX is a well-known chemical propellant. The solid phase of HMX consists of three polymorphs [2–4] and a hemihydrate [5] in which differences exist in the ring conformation [5–10]. The structure and scheme of polymorphism of OHMX are not known and were determined in this work. The enthalpy changes and solid–solid phase transition kinetic parameters were measured for comparison with those of HMX [10–17]. The decomposition products from slow and fast heating were determined by rapid-scan infrared methods [18]. The fast decomposition studies attempt to similate, in so far as possible, conditions that initiate combustion. Although OHMX is found to be somewhat less thermally stable than HMX, the products and their concentration as a function of pressure lead to the conclusion that the reactivity of these analogous linear and cyclic nitramines is similar.

EXPERIMENTAL

A sample of OHMX [19] was provided by George Nauflett (NSWC). Both HMX and OHMX are strongly energetic materials. The IR spectra were recorded on a Nicolet 60SX FTIR spectrometer employing an HgCdTe-B detector. Differential thermal analyses were conducted on a Mettler 2000B analyzer.

Polymorphism of OHMX was studied on samples precipitated from DMF, acetone, acetonitrile, ethanol, and diethylether. Fast evaporation of the solvent (20 ml min^{-1}) at room temperature using a vigorous stream of N_2 resulted in a polycrystalline powder of OHMX(IV) for all solutions except the less volatile DMF solution. Crystals of OHMX(III) were grown from a slowly evaporated acetone solution, while crystals of OHMX(II) were obtained by slow evaporation of a DMF solution. No other polymorphs could be synthesized by variations on these methods. Two procedures were

used to apply solid OHMX to the NaCl plates for the purpose of recording high-quality transmission IR spectra. In one, 1–2 mg of OHMX(I), (II) and (III) were spread on the plate and pressed and burnished with a micro-spatula until the surface was glossy. The spectrum obtained was essentially scatter-free. Alternatively, 1–2 mg of OHMX(II) or (III) were placed on the NaCl plate and a trace of DMF or ethanol was added. The paste was ground with the microspatula using a circular motion and then evenly and thinly spread on the plate. The solvent was then evaporated. The solvent addition and grinding procedure was continued until a good spectrum was obtained. The polymorphs of HMX were synthesized as described elsewhere [3,10]. High-quality spectra of α-, β-, and γ-HMX were obtained after burnishing an ethanol paste of each polymorph on an NaCl plate. In all cases care must be exercised to avoid inducing phase transitions due to the friction.

Homebuilt, variable-temperature IR cells were employed to study the phase transitions of OHMX. The heating rate was $\leqslant 5$ K min^{-1}. Kinetic measurements on OHMX(III → IV) were conducted on neat samples of OHMX in a cell [20] maintained at a constant temperature by an Omega temperature controller and whose temperature was measured on a Fluke

TABLE 1

Crystallographic data for $C_5H_{12}N_8O_8$, OHMX

(a) *Crystal data*			
crystal system	monoclinic	Z	4
space group	$P2_1/c$	μ (cm^{-1}) (MoK_α)	1.39
a (Å)	20.952(7)	D (calc) (g cm^{-3})	1.598
b (Å)	9.477(2)	cryst. dim. (mm)	0.31×0.31×0.31
c (Å)	6.571(2)	cryst. color	colorless
β (deg)	96.29(3)	temp. (K)	296
V (Å^3)	1296.8(7)	F(000)	648
(b) *Data collection*			
diffractometer	Nicolet R3m/μ	std rflns	3 stds/97 rflns
radiation	MoK_α (λ = 0.71073 Å)	decay (%)	<1
monochromator	graphite	rflns collected	2389
scan method	$\theta/2\theta$	unique rflns	2033
2θ limits (deg)	$4 \leqslant 2\theta \leqslant 48$	R(int) (%)	0.99
scan speed (deg min^{-1})	var. 5–20	unique rflns $F_0 \geqslant 3\sigma(F_0)$	1634
(c) *Refinement*			
R_F, R_{wF} (%)	3.84, 4.68	Δ/σ	0.04
g ($\omega^{-1} = \sigma^2(F_0) + gF_0^2$)	0.001	Δ_ρ (e Å^{-3})	0.19
GOF	1.301	data/param.	8.6

[a] Obtained from a least-squares best fit of the angular settings of 25 reflections, $21° \leqslant 2\theta \leqslant 25°$.

digital thermometer. Thirty-two scans at 2 cm^{-1} resolution were accumulated for each spectrum. The intensity values ($I - I_\infty$) of well-separated peaks of OHMX(III) (1515 and 1252 cm^{-1}) were then measured as a function of time. Because of the difficulties with heat transfer, some imprecision can be incurred which is best represented by the error bars when ln k is plotted against $1/T$ (see text). At least seven intensity measurements covering a wide range of intensity values were recorded at each of seven temperatures between 383 and 395 K.

The rapid-scan infrared methods and quantitation process for the high-rate thermolysis studies on 1-mg samples have been described fully elsewhere [18]. The analysis is performed in real-time while the gas products are evolved from an electrically heated nichrome ribbon filament into an Ar atmosphere. Spectra at 4 cm^{-1} resolution were recorded at a rate of 10 scans s^{-1}. H_2O was not quantified because of its complicated rotation–vibration fine structure. IR-inactive products were also not quantified.

In the determination of the crystal structure of OHMX(II), preliminary photographic characterization of crystals of OHMX(II) grown from DMF solution showed $2/m$ Laue symmetry and were of good quality. Systematic absences in the diffraction data uniquely identified the space group as

TABLE 2

Atomic coordinates ($\times 10^4$) and isotropic thermal parameters ($Å^2 \times 10^3$)

	x	y	z	U [a]
O(1)	4342(1)	7053(2)	−3890(3)	78(1)
O(2)	3347(1)	7010(2)	−3220(3)	69(1)
O(3)	3917(1)	3794(2)	1570(3)	57(1)
O(4)	3125(1)	4663(2)	3079(2)	63(1)
O(5)	1930(1)	3772(2)	−2854(3)	63(1)
O(6)	1140(1)	3408(2)	−975(3)	61(1)
O(7)	1585(1)	7665(2)	1314(2)	50(1)
O(8)	604(1)	7832(2)	2128(3)	67(1)
N(1)	3968(1)	5177(2)	−2395(3)	41(1)
N(2)	3090(1)	4779(2)	−286(3)	35(1)
N(3)	1943(1)	4821(2)	163(3)	38(1)
N(4)	1046(1)	5721(2)	1895(3)	42(1)
N(5)	3884(1)	6483(2)	−3229(3)	52(1)
N(6)	3396(1)	4395(2)	1548(3)	42(1)
N(7)	1651(1)	3951(2)	−1308(3)	45(1)
N(8)	1079(1)	7147(2)	1796(3)	43(1)
C(1)	4571(1)	4456(3)	−2634(4)	61(1)
C(2)	3388(1)	4396(2)	−2114(3)	38(1)
C(3)	2505(1)	5615(2)	−316(3)	35(1)
C(4)	1654(1)	4968(2)	2069(3)	40(1)
C(5)	484(1)	5089(3)	2670(4)	63(1)

[a] Equivalent isotropic U defined as one-third of the trace of the orthogonalized U_{ij} tensor.

TABLE 3

Bond lengths and angles for OHMX(II)

Bond lengths (Å)			
O(1)–N(5)	1.222(3)	O(2)–N(5)	1.231(3)
O(3)–N(6)	1.230(2)	O(4)–N(6)	1.234(2)
O(5)–N(7)	1.238(3)	O(6)–N(7)	1.228(2)
O(7)–N(8)	1.240(2)	O(8)–N(8)	1.228(2)
N(1)–N(5)	1.358(3)	N(1)–C(1)	1.460(3)
N(1)–C(2)	1.452(3)	N(2)–N(6)	1.351(2)
N(2)–C(2)	1.459(3)	N(2)–C(3)	1.459(2)
N(3)–N(7)	1.364(2)	N(3)–C(3)	1.459(2)
N(3)–C(4)	1.456(3)	N(4)–N(8)	1.355(3)
N(4)–C(4)	1.454(3)	N(4)–C(5)	1.462(3)
Bond angles (deg)			
N(5)–N(1)–C(1)	117.3(2)	N(5)–N(1)–C(2)	116.3(2)
C(1)–N(1)–C(2)	121.4(2)	N(6)–N(2)–C(2)	117.6(2)
N(6)–N(2)–C(3)	118.3(2)	C(2)–N(2)–C(3)	124.0(2)
N(7)–N(3)–C(3)	118.0(2)	N(7)–N(3)–C(4)	118.1(2)
C(3)–N(3)–C(4)	123.9(2)	N(8)–N(4)–C(4)	116.3(2)
N(8)–N(4)–C(5)	118.2(2)	C(4)–N(4)–C(5)	120.3(2)
O(1)–N(5)–O(2)	125.2(2)	O(1)–N(5)–N(1)	118.3(2)
O(2)–N(5)–N(1)	116.5(2)	O(3)–N(6)–O(4)	124.9(2)
O(3)–N(6)–N(2)	118.0(2)	O(4)–N(6)–N(2)	117.1(2)
O(5)–N(7)–O(6)	126.0(2)	O(5)–N(7)–N(3)	116.7(2)
O(6)–N(7)–N(3)	117.3(2)	O(7)–N(8)–O(8)	124.7(2)
O(7)–N(8)–N(4)	117.2(2)	O(8)–N(8)–N(4)	118.1(2)
N(1)–C(2)–N(2)	114.6(2)	N(2)–C(3)–N(3)	114.5(2)
N(3)–C(4)–N(4)	115.0(2)		

$P2_1/c$. Table 1 provides other crystal, data collection, and refinement parameters. Corrections for *Lp* effects, but not absorption, were applied to the intensity data. A profile-fitting procedure was used to improve the precision in the measurement of weak reflections.

The structure was straightforwardly solved by direct methods. All non-hydrogen atoms were refined with anisotropic temperature factors, and hydrogen atoms were placed in idealized locations as updated, isotropic contributions, but not refined (d(C–H)=0.96 Å).

SHELXTL (ver. 5.1) software was used for all computations (Nicolet Corp., Madison, WI). Table 2 provides the non-hydrogen atom atomic coordinates, and Table 3 the bond distances and angles. Observed and calculated structure factors, H atom coordinates, and anisotropic thermal parameters are available as supplementary material from the authors.

Structure of OHMX

A projection of the OHMX molecule in one of its polymorphs is shown in Fig. 1. The C(3) atom lies on an approximate, non-crystallographically

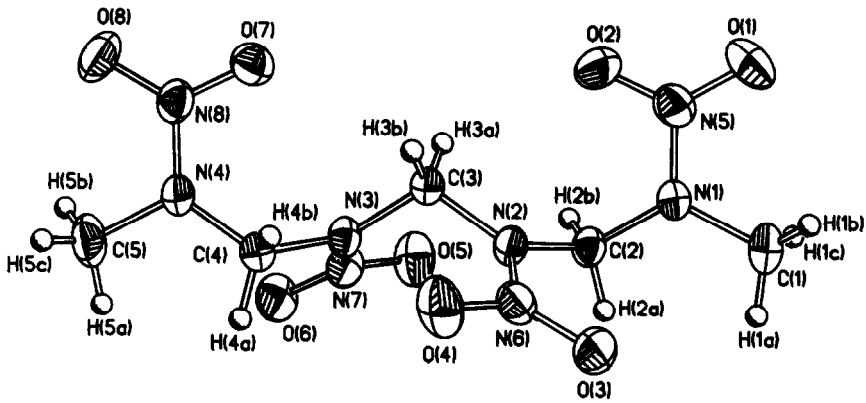

Fig. 1. Molecular structure and labeling scheme for OHMX in crystalline phase II.

imposed, two-fold axis, the symmetry of which can also be visualized in the orthogonal projection shown in Fig. 2. The geometry of the chain is based on repeating CH_2NNO_2 units positioned at about 120° intervals about a long axis so as to define a helix. The non-bonded intramolecular contacts and the interatomic distances are comparable to those of the polymorphs of HMX [21]. The two inner aza-nitrogen atoms tend toward planarity (sum of the angles is 359–360°) whereas the two outer aza-nitrogen atoms are slightly distorted toward pyramidal geometry (355°). Distortions of this type are typical of nitramine molecules. This difference does not translate into any systematic variation in the N–N bond distances which fall into the

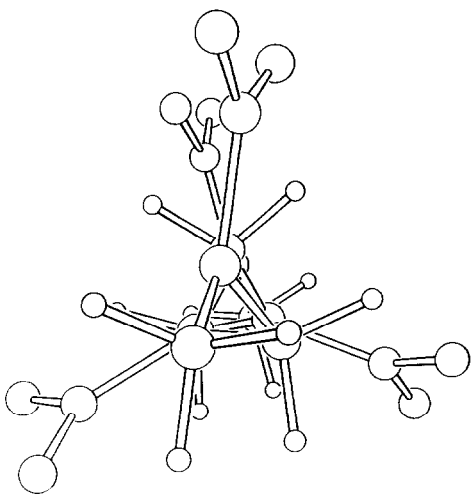

Fig. 2. End view of the OHMX molecule depicting the helical nature of the backbone and the pseudo two-fold axis involving C(3).

TABLE 4

Intermolecular heavy atom distances ($\leqslant 3.25$ Å) and the shortest CH $\cdots$ O distance in OHMX(II)

$x, y, -1+z$	$x, 1.5-y, -0.5+z$
C(2) $\cdots$ O(4) 3.157	N(8) $\cdots$ O(8) 3.120
N(5) $\cdots$ O(4) 3.247	C(3) $\cdots$ O(7) 3.215
$x, 1.5-y, 0.5-z$	$-x, -0.5+y, 0.5-z$
N(8) $\cdots$ O(7) 3.046	C(5) $\cdots$ O(8) 3.139
C(3) $\cdots$ O(2) 3.090	
N(5) $\cdots$ O(1) 3.221	$x, 0.5-y, 0.5+z$
H(3B) $\cdots$ O(2) 2.288	O(6) $\cdots$ O(5) 3.235

range of 1.351–1.364(3) Å. Such bond distances are qualitatively expected to produce $\nu_{as}(NO_2)$ in the range of 1530–1550 cm^{-1} in the IR spectrum [22]. The average value of 1555 cm^{-1} observed experimentally is an acceptable connection in context. Perhaps the presence of the CH_3 rather than a CH_2 group attached to the NNO_2 unit slightly perturbs this correlation.

The molecular packing of the crystal lattice incorporates pairwise interactions of the NO_2 groups in adjacent molecules reminescent of dipolar interactions involving each N–O unit [21,23]. Table 4 lists the intermolecular heavy atom interactions that lie within a radius of 3.25 Å of each atom. None are strong associations based on the Van der Waals distances and all but O(2) $\cdots$ O(5) can be regarded as attractions on the basis of the expected electrostatic charge distribution in nitramines [24]. One marginally important intermolecular C–H $\cdots$ O "hydrogen bond" with an O $\cdots$ H distance of 2.29 Å is present. Overall, the number of intermolecular interactions at $\leqslant 3.25$ Å in OHMX is about one-half the number in the cyclic nitramine analogues [21]. In accordance, the density of OHMX is 1.60 g cm^{-3} whereas the HMX polymorphs are 1.78–1.90 g cm^{-3} [3–6]. Also, OHMX melts at 487 K which is about 65° below the liquefaction temperature of HMX.

Solid–solid phase transformations

Solid–solid phase transitions can influence the efficacy of energetic materials because the density can change and crystal stress and fracturing may occur. The cyclic nitramine, HMX, exhibits rich polymorphism and considerable flexibility in the ring conformation [2–10]. Likewise, considerable flexibility could exist in OHMX leading to versions of the molecule having approximately the same intramolecular distances as the polymorph structurally characterized above. Small differences in the crystal lattice packing should be possible as well given the complicated electrostatic

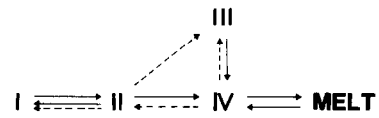

Fig. 3. Phase transition scheme of OHMX. OHMX(V) (not shown) is a premelt phase. The solid lines represent thermally induced transitions while the dashed lines represent friction-induced transitions. The transition temperature ranges are given in Table 6.

exterior of the molecule. Indeed, OHMX exhibits a considerable variety of solid phases.

A careful study was conducted of the mid-IR spectra and differential thermal analysis of neat samples of OHMX grown from different solvents as a function of temperature. While other polymorphs might be obtained from solvents not tested and under pressure, the scheme shown in Fig. 3 is a reasonably complete picture of polymorphism for OHMX under common conditions. Fast evaporation of all solutions examined produced OHMX(IV) as a fine powder. OHMX(II) was obtained by slow evaporation of a DMF solution while OHMX(III) was obtained by slow evaporation of an acetone solution or by mechanical friction on OHMX(II). OHMX(I) formed when finely dispersed OHMX(II) or OHMX(IV) on an NaCl plate was subjected to mechanical friction or when warm OHMX(II) was cooled to room temperature. Polymorphs I–IV are stable at room temperature for a reasonable duration of time. Large thermal hysteresis allows OHMX(IV), which was produced only upon heating of OHMX(I), (II) or (III), to be supercooled to room temperature. The pre-melt phase, OHMX(V), is nearly thermally neutral with respect to OHMX(IV) according to DTA. Line-broadening in the IR spectrum of OHMX near the melting point precludes detection of OHMX(V) by the internal modes of the molecule. No phase transitions in OHMX were evident in the mid-IR absorptions or DTA from 153 to 273 K.

The aforementioned crystal structure determination applies to OHMX(II). Efforts to grow suitable crystals of the other polymorphs were unsuccessful, although thin plates of OHMX(III) were grown from acetone solution. These proved to be not only too small in one dimension, but also hopelessly twinned. Consequently, concrete structural details are available only for OHMX(II).

In the absence of X-ray crystallographic data, the IR spectra provide general information on what is taking place in the other polymorphs. Figure 4 compares the internal modes (700–3100 cm^{-1}) of polymorphs I, II, III, and IV of OHMX at 298 K and the melt phase at 493 K. Table 5 summarizes the mid-IR frequencies. A surprising feature is the similarity of the low-temperature phase, OHMX(I), and the melt phase. Normally, a solid phase whose IR spectrum has the appearance of OHMX(I) would be

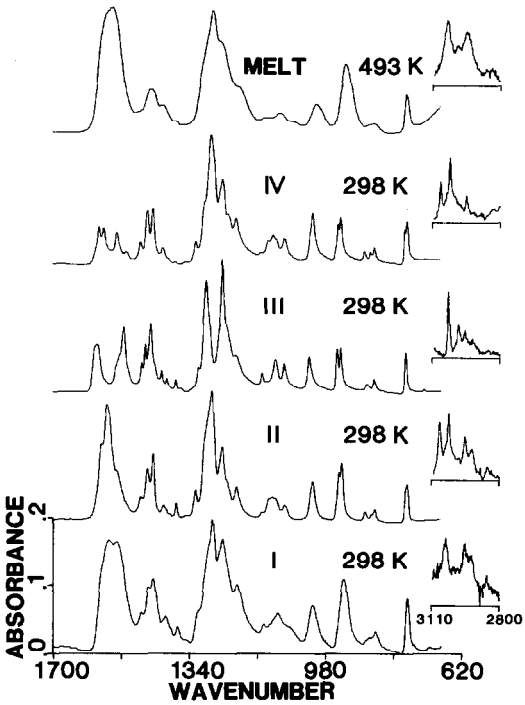

Fig. 4. Absorbance mode mid-IR spectra of pure samples OHMX(I) to OHMX(IV) and the melt phase. OHMX(V) (not shown) is indistinguishable from OHMX(IV). The methylene/methyl region is shown in the insert. Thirty-two scans at 2 cm^{-1} resolution were collected.

expected to occur near the melting point and to originate from disorder. This is the case with several other nitramines recently studied: 1,3,5,7-tetranitro-3,7-diazabicyclo[3.3.1]nonane [25], 3,7-dinitro-1,3,5,7-tetrazabicyclo[3.3.1]nonane [25], and 1,4-dinitrofurazano [3,4-b]piperazine [1]. The similarity of OHMX(I), a lower temperature phase, to the melt phase spectrum is therefore unexpected. That the broad lines of OHMX(I) might result from a physical mixture of two or more polymorphs can be ruled out from the appearance of the CH_2 region. The fact that both the IR and DTA methods demonstrate a reversible phase transition between OHMX(I) and (II) attests to OHMX(I) being a structurally unique phase. Disorder, or at least the existence of multiple, crystallographically independent molecules in the unit cell, remains the most plausible explanation for the broad absorptions of OHMX(I) and its spectral similarity to the melt phase. This disorder may originate from the intrinsic difficulty that globular molecules, such as OHMX, have in organizing.

The splitting of $\nu_{as}(NO_2)$ in OHMX(III) is quite distinctive indicating that a greater difference exists among the NO_2 groups than is present with

TABLE 5

Mid-IR frequencies (cm^{-1}) for OHMX

I (298 K)	II (298 K)	III (298 K)	IV (298 K)	Melt (493 K)	Suggested assignments
	3074 w		3073 w		
3042 w	3032 w	3033 w	3030 w	3041 w	$\nu_{as}(CH_2)$ and (CH_3)
2992 vw		2989 w		2993 vw	
2955 w	2958 w	2959 w	2955 w	2952 w	
2928 w	2925 w	2925 vw			$\nu_s(CH_2)$ and (CH_3)
2854 vw	2855 vs			2847 vw	
	1573 s,sh	1585 m	1579 m		
1553 vs	1561 vs		1566 m		
1532 vs	1533 m,sh	1530 m,sh	1531 m	1542 vs	$\nu_{as}(NO_2)$
		1515 s	1505 w		
1468 m	1467 m	1466 m	1468 m		
1449 m	1451	1457 m	1450 s	1442 m	$\delta_{as}(CH_3)$
1436 s	1436 s	1443 s	1436 s		
1404 m	1408 w	1414 w	1409 w	1410 w	$\delta(CH_2)$
	1391 vw	1400 w			
1373 w	1374 w	1376 w	1374 vw	1373 vw	$\delta_s(CH_3)$
1352 wv	1346 vw	1363 vw	1346 vw		
1318 m,sh	1324 m	1315 w,sh	1322 m		
1294 s,sh	1294 vs,sh	1295 vs	1295 m,sh		$\nu_s(NO_2)$
1279 vs	1280 vs		1280 vs	1275 vs	
1252 vs	1253 s	1252 vs	1251 s	1255 s,sh	
	1239 m,sh	1240 m,sh	1237 m,sh		
1214 m	1215 m	1216 m,sh	1215 m	1209 m,sh	ν(N–N)
1143 w	1146 w	1148 w	1148 vw		
			1130 w	1134 vw	
1107 m	1118 m	1112 m	1117 m	1096 w	ν(C–N)
1076 w,sh	1087 w	1089 m	1086 m	1063 vw	
1015 m	1014 m	1024 m	1013 s	1002 m	
	945 s	950 m	946 m,sh		CN rocking
933 s	937 s	940 m	939 m	925 s	
	875 w	870 w	875 w		
862 w,sh	857 w,sh		860 w		
849 w	850 w	852 w	849 w	848 w	
	767 m,sh	769 m	769 m,sh		$\delta(NO_2)$
765 m	764 m		763 m	764 m	
703 vw		718 vw			

OHMX(II). Unfortunately, this difference could not be substantiated by X-ray crystallography owing to the aforementioned difficulties. OHMX(II) and OHMX(IV) appear to be more structurally similar to one another than OHMX(III) is to any other polymorph.

Despite some marked spectral differences, it does not appear that a major change in the conformation of the OHMX molecule takes place during any phase transition. This conclusion is fortified by comparing the spectra of the

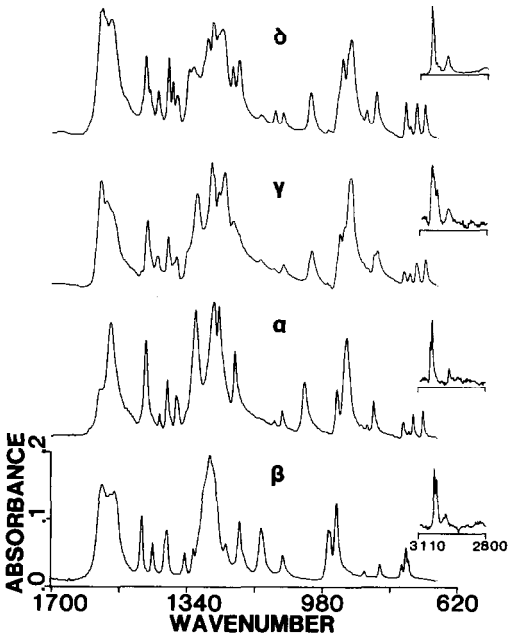

Fig. 5. Absorbance mode mid-IR spectra of pure samples of the four polymorphs of HMX and the γ-form which is a hemihydrate.

polymorphs of OHMX to those of HMX, which are shown in Fig. 5. The HMX molecule in the β-polymorph adopts the chair–ring conformation [6] while α-, γ-, and δ-HMX are known to be comprised of molecules in the chair–chair-ring conformation [5–10]. Consequently, the IR spectrum of β-HMX is distinct from the spectra of the others. The spectra of the OHMX polymorphs are not so radically different from one another which suggests that the chain conformation is similar in all polymorphs.

The enthalpy changes for the phase transitions of OHMX are given in Table 6. Their magnitude is comparable to those of HMX (0.7–2.2 kcal mol^{-1}) [11–15] probably because of the similar functional groups and molecular weights of these two molecules. However, in practice solid–solid phase transitions are often influenced more by kinetic considerations than

TABLE 6

Enthalpy changes for the solid–solid phase transitions of OHMX

Transition	ΔH (kcal mol^{-1})	Center temp. (K) DTA	Temp. range (K) IR
OHMX(I ⇄ II)	0.89	289	309–323
OHMX(II → IV)	3.40	427	423–463
OHMX(III → IV)	1.17	387	403–419
OHMX(IV → V)	0.09	480	–

thermodynamic factors. A kinetic investigation of OHMX(III → IV) was, therefore, undertaken. This transformation is sluggish and takes place over a broad temperature range making it well suited for rate studies by IR spectroscopy. For instance, the transformation is complete in about 180 min at 383 K and 45 min at 394 K. The HMX ($\beta \rightarrow \delta$) transformation which has been similarly studied in the vicinity of 458 K is considerably faster [16]. We feel that the faster rate for HMX can be attributed mostly to the higher phase transition temperature.

During the OHMX(III → IV) transformation, a significant change in the intensity of $\nu_{as}(NO_2)$ at 1515 cm^{-1} and $\nu_s(NO_2)$ at 1252 cm^{-1} occurs that can be used for rate constant calculations. The change in the absorbance of these modes produces the same rate constant for an isothermal run at 392 K (e.g. $\ln k = 7.2 \pm 0.2$), indicating that the change in the spectrum is produced by a change in the molecular or crystal structure rather than by a more etherial variable such as vibrational coupling. The first-order rate equation (1) was used to compute rate constants at seven temperatures. Equation (2) was used to calculate the activation energy, E_a, and the frequency factor, A.

$$\ln \frac{[\text{OHMX(III)}]_t}{[\text{OHMX(III)}]_0} = -kt \tag{1}$$

$$\ln k = \ln A - E_a/RT \tag{2}$$

A plot of eqn. (2) is shown in Fig. 6. $E_a = 50.8$ kcal mol^{-1} while $\ln A = 58.1$. The frequency factor for solid-state reactions has dubious meaning in the context of how it is viewed in gas and solution phase chemistry [26].

The first-order kinetics of this transformation in OHMX and the transformations in HMX corresponds to $n = 1$ in the Avrami equation [27]. Such a

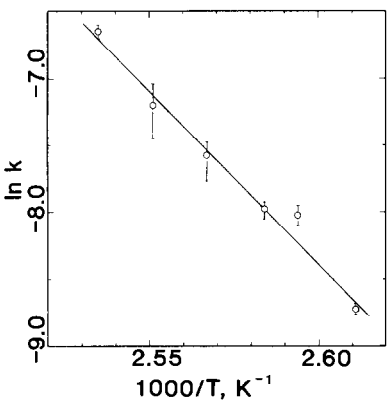

Fig. 6. Arrhenius plot of the rate constants for the OHMX(III → IV) solid–solid phase transformation.

kinetic expression is believed to originate from a rate that is initiated by nucleation and regulated by continuing nucleation at the grain boundaries [27]. The spectrum, therefore, measures the statistical ensemble of particles undergoing these events. The activation energy of OHMX(III → IV) is essentially the same as those for the thermally induced phase transitions of HMX (48.4–52.3 kcal mol^{-1}) [16] despite the fact that the transition temperature and molecular details differ. This suggests that the IR method mostly measures nucleation kinetics. Fifer [17] arrived at the same conclusion after studying HMX($\beta \rightarrow \delta$) on individual particles by DSC methods. DSC appears to measure the propagation kinetics of HMX for which E_a is much smaller [17].

The large activation energy for nucleation is probably responsible for the sluggishness of the reconstructive phase transitions in polycrystalline HMX and OHMX. The similarity of values of E_a suggests that the physical and molecular properties controlling the nucleation of the phase transitions in these compounds are essentially the same. The other phase transformations, OHMX(I ⇆ II) and OHMX(II → IV), were not studied because of the absence of intense, well-separated absorptions that can be used to measure the kinetic constants.

Thermal decomposition

On the basis of the N–N bond distances, OHMX is predicted [22] to liberate NO_2 by N–N bond homolysis, but to do so in strong competition with reactions involving the backbone which liberate products such as HCN, N_2O and CH_2O. It has been noted with other nitramines that the presence of the fragment

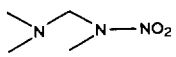

usually leads to N_2O and CH_2O upon thermolysis [25]. HMX is expected to [22] and does [18] behave similarly. Figures 7 and 8 show the effect of pressure on the initial concentration (first 0.2 s) of the IR-active gas products, excluding H_2O, when OHMX and HMX are heated at about 110 K s^{-1}. These data were acquired by conducting a separate thermolysis experiment at each static Ar gas pressure. Common products are liberated by HMX and OHMX except that HONO is produced by HMX [18], but not OHMX, while CH_4 is produced by OHMX, but not HMX. CH_4 from OHMX is expected because parent molecules containing the CH_3 groups frequently liberate CH_4 [28,29]. OHMX is a rare example of a nitramine that does not produce HONO [30].

The high degree of reactivity of NO_2 and CH_2O causes a fast drop-off in their initial concentration as a function of increasing time (Fig. 9) and pressure. At lower pressure (see Figs. 7 and 8) the concentrations of the

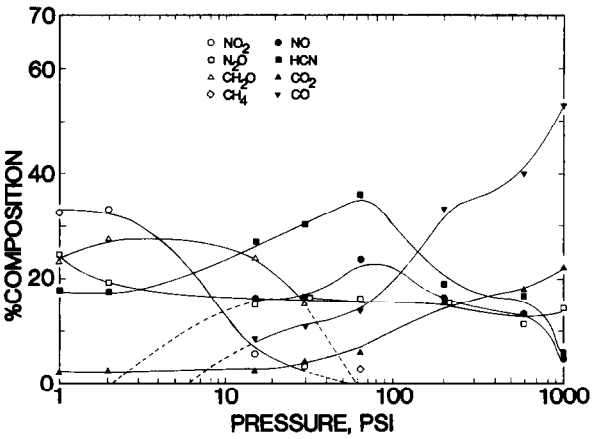

Fig. 7. Pressure dependence of the initial gas products (first 0.2 s), excluding H_2O and the IR-inactive products, from the thermolysis of OHMX in an Ar atmosphere at each pressure using $dT/dt = 110$ K s^{-1}.

reactive decomposition products are relatively high. As the pressure increases, the concentration of secondary and later reaction products (NO, CO, CO_2) builds at the expense of the more reactive products (NO_2, CH_2O). At the higher pressures, the combustion products CO, CO_2 and H_2O (not shown), no doubt along with N_2, are the dominant products. This pattern can be explained by the pressure-induced shift in the balance for reactions that occur among the gas-phase species and between the gas and condensed phases [18]. At low pressure the reactive gases diffuse away from the

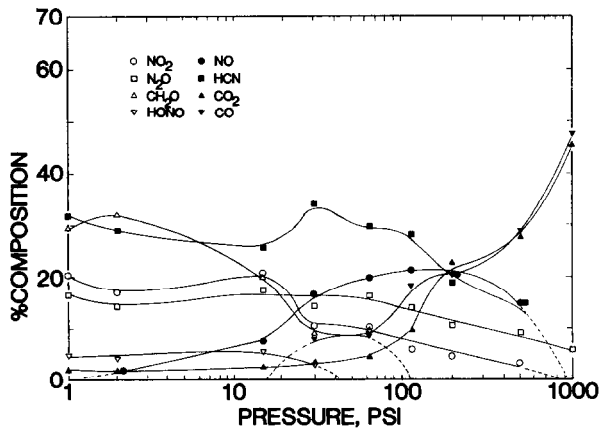

Fig. 8. Pressure dependence of the initial gas products (first 0.2 s), excluding H_2O and the IR-inactive products, from the thermolysis of HMX in an Ar atmosphere at each pressure using $dT/dt = 110$ K s^{-1}.

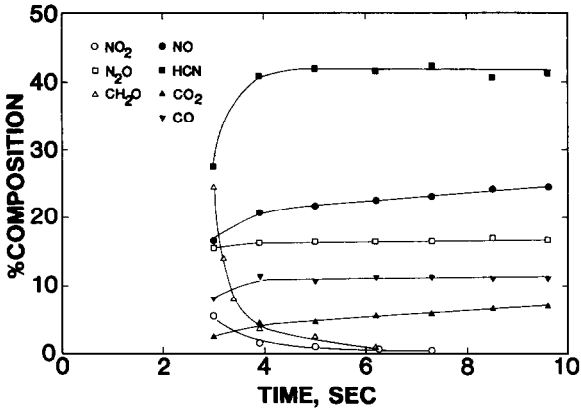

Fig. 9. Concentration vs. time dependence of the thermolysis products of OHMX (excluding H_2O and the IR-inactive products) at 15 psi Ar using a heating rate of 100 K s^{-1}. The most reactive products (CH_2O and NO_2) are highly time-dependent owing to extensive secondary reaction chemistry.

condensed phase and from one another so that the second-stage reactions are less extensive. As the pressure increases, an intermediate class of decomposition products prevails owing to the large number of secondary reactions. At the highest pressure the course of these later-stage reactions progress so far that only the products of combustion are detected.

An evaluation of the relative stability of HMX and OHMX can be obtained by comparing the IR spectra of a slowly heated thin film of the sample. The spectrum of solid OHMX heated at 5 K min^{-1} through the decomposition point reveals that OHMX melts at about 490 K but gives no evidence of decomposition until about 500 K. HMX begins to decompose in the solid phase below its liquefaction temperature of about 550 K [31]. Thus, OHMX appears to be somewhat less thermally stable than HMX. DTA data on a comparable pair of cyclic and open-chain nitramines suggest that there is little difference in their thermal stability [32]. This latter conclusion appears not to be completely general. On the other hand, once the decomposition temperature is reached the rate of decomposition of OHMX is slower than HMX, which is consistent with observations made before [33] about the decomposition rates of analogous linear and cyclic nitramines.

The residue from slow decomposition of OHMX produces an IR spectrum resembling that produced by HMX [31]. The most intense absorptions at 1690 and 1749 cm^{-1} suggest the presence of an amide and/or an alkylammonium species [31].

In summary, although OHMX is less thermally stable than HMX, its rate of decomposition at the decomposition point is lower. The stable, small molecule products liberated from HMX and OHMX are similar. Reaction sequences involving competitive C–N and N–N bond fission take place as is

predicted by the IR spectrum and the bond distances. In the solid phase HMX and OHMX both exhibit extensive polymorphism. The similar composition and molecular electrostatics appear to be responsible for the similarity in the thermodynamic and kinetic parameters for the nucleation of their solid–solid phase transitions.

ACKNOWLEDGMENTS

We are grateful to Dr. George Nauflett (NSWC) for providing a sample of OHMX. We also wish to thank the Air Force Office of Scientific Research, Aerospace Sciences, for supporting these studies.

REFERENCES

1 For paper 16 in this series see Y. Oyumi, A.L. Rheingold and T.B. Brill, J. Phys. Chem., 90 (1986) 4686.
2 A.S. Teetsov and W.C. McCrone, Microsc. Cryst. Front., 15 (1965) 13.
3 H.H. Cady and L.C. Smith, LAMS-2652, Los Alamos Scientific Lab., 3 May 1962.
4 W.C. McCrone, Anal. Chem., 22 (1950) 1225.
5 P. Main, R.E. Cobbledick and R.W.H. Small, Acta Crystallogr., Sect. C, 41 (1985) 1351.
6 H.H. Cady, A.C. Larson and D.T. Cromer, Acta Crystallogr., 16 (1963) 617.
7 C.S. Choi and H.P. Boutin, Acta Crystallogr., Sect. B, 26 (1970) 1235.
8 R.E. Cobbledick and R.W.H. Small, Acta Crystallogr., Sect. B, 30 (1974) 1918.
9 A.G. Landers, T.M. Apple, C. Dybowski and T.B. Brill, Magn. Reson. Chem., 23 (1985) 158.
10 F. Goetz and T.B. Brill, J. Phys. Chem., 83 (1979) 340.
11 P.G. Hall, Trans. Faraday Soc., 67 (1971) 556.
12 G. Krien, H.H. Licht and J. Zierath, Thermochim. Acta, 6 (1973) 465.
13 J. Rylance and D. Stubley, Thermochim. Acta, 13 (1975) 253.
14 A.G. Landers and T.B. Brill, J. Phys. Chem., 84 (1980) 3573.
15 R.J. Karpowicz and T.B. Brill, AIAA J., 20 (1982) 1586.
16 T.B. Brill and R.J. Karpowicz, J. Phys. Chem., 86 (1982) 4260.
17 R.A. Fifer, Proc. 19th JANNAF Combust. Meet., CPIA Publ. 366, Greenbelt, MD, Oct. 1982, p. 311.
18 Y. Oyumi and T.B. Brill, Combust. Flame, 62 (1985) 213.
19 J. Denkstein and V. Kaderbeck, Collect. Czech. Chem. Commun., 31 (1966) 2904.
20 R.J. Karpowicz and T.B. Brill, Appl. Spectros., 37 (1983) 79.
21 T.B. Brill and C.O. Reese, J. Phys. Chem., 84 (1980) 1376.
22 T.B. Brill and Y. Oyumi, J. Phys. Chem., 90 (1986) 2679.
23 A.J. Landers, T.B. Brill and R.A. Marino, J. Phys. Chem., 85 (1981) 2618.
24 J. Stals, Aust. J. Chem., 22 (1969) 2505.
25 Y. Oyumi, T.B. Brill and A.L. Rheingold, J. Phys. Chem., 90 (1986) 2526.
26 R.A.W. Hill, in J.H. De Boer (Ed.), Reactivity in Solids, Elsevier, New York, 1961, pp. 294, 91.
27 C.N.R. Rao and K.J. Rao, Phase Transitions in Solids, McGraw-Hill, New York, 1978, pp. 91–95.

28 Y. Oyumi and T.B. Brill, Combust. Flame, 65 (1986) 103.
29 Y. Oyumi and T.B. Brill, Combust. Flame, 65 (1986) 127.
30 T.B. Brill and Y. Oyumi, J. Phys. Chem., in press.
31 R.J. Karpowicz and T.B. Brill, Combust. Flame, 56 (1984) 317.
32 Y.P. Carignan and D.R. Satrianna, J. Org. Chem., 32 (1967) 285.
33 W.H. Jones, J. Am. Chem. Soc., 76 (1954) 928.